

Effects of open field line plasma on rotating magnetic field current drive in a field-reversed configuration

Richard D. Milroy

University of Washington, Redmond Plasma Physics Laboratory, 147700 NE 95th Street, Redmond, Washington 98052

(Received 3 January 2001; accepted 6 March 2001)

A numerical model has been used to study the effects that open field line plasma may have on the rotating magnetic field (RMF), when it is applied to a field-reversed configuration (FRC) for current drive. The model is a two-dimensional ($r-\theta$) magnetohydrodynamic computer simulation. The RMF is found to be an extremely good particle *pump*, continuously sweeping plasma into the FRC from the outer region, and thus evacuating the space near the containment vessel wall. This effect can lead to a very low density near the wall, providing good thermal insulation. However, if there is a plasma source in the open field line region (such as outgassing from the containment vessel wall) capable of maintaining relatively low-density plasma, the RMF may be amplified in this region. While this effect may speed the rate of penetration, it also has a deleterious effect where excessive penetration leads to predictions of an internal structure that rotates slower than the RMF, and chaotic equilibrium. © 2001 American Institute of Physics. [DOI: 10.1063/1.1368140]

I. INTRODUCTION

A transverse rotating magnetic field (RMF) is being investigated as a current drive mechanism for the field-reversed configuration (FRC). Much of the pioneering work for this RMF current drive was performed by Jones and co-workers, and has been summarized in a recent review article.¹ Much of this work employed a device known as a rotamak, which normally has significant plasma pressure on the containment vessel wall. More recent experiments at the University of Washington^{2,3} employ flux-conserving coils where the external field naturally increases when the FRC expands radially. This permits the separatrix position to be controlled, and thus ensures that it is inside the tube wall. Experiments, and numerical modeling⁴ have both found that when the separatrix is inside the containment vessel wall, RMF action sweeps the open field-line plasma inward, leading to an extremely low plasma density beyond the separatrix.

In previous numerical magnetohydrodynamic (MHD) studies,⁴ the separatrix radius was inside, but very close to the containment vessel wall. In this paper, the same numerical model is used to explore the case where the separatrix radius is further from the containment vessel wall, leaving a significant open field line region that may contain low-density plasma. It is found that the RMF acts as a very efficient particle pump, which continuously sweeps the plasma from this region into the FRC. This can leave an extremely low-density region near the vessel wall. However, if a plasma source exists that maintains the plasma density in the open field line region above a critical (but low) value, the RMF field magnitude is amplified in the open field line region, and thus increases with decreasing radius, between the wall and the FRC. This effect can greatly reduce the penetration time for the RMF, but it can also cause the RMF to penetrate too far. Then the torque required to maintain the

current exceeds the capability of the RMF field near the wall, leading to an internal magnetic structure that rotates slower than the RMF. This generates to a chaotic *equilibrium*, which is not at all desirable.

In Sec. II we review the expected RMF profile in the region between the FRC separatrix and the plasma tube wall based on a vacuum solution. This is compared with a numerically calculated profile, and it is shown that the presence of low-density plasma can significantly affect the solution. A physical explanation for these results is then offered. A summary and discussion of the implications of this effect is discussed in Sec. III.

II. OPEN FIELD LINE EFFECTS

A. Vacuum solution

Before exploring the effects of the plasma in the region between the FRC separatrix and the vessel wall, we will examine the vacuum solution for the RMF field. In a vacuum, the RMF can be represented with the z -component of the vector potential, A_z .^{4,5} If the vacuum exists in the region $r > R$, A_z must satisfy the equation

$$\nabla^2 A_z = 0, \quad r \geq R. \quad (1)$$

The solution to this equation⁵ can be expressed as

$$A_z = \sum_n A_{z,n} e^{in\theta},$$

where

$$A_{z,n} = \alpha_n r^n + \beta_n r^{-n}, \quad (2)$$

$$B_\theta = -\frac{\partial A_z}{\partial r} = -\sum_n (n\alpha_n r^{(n-1)} - n\beta_n r^{-(n+1)}) e^{in\theta}. \quad (3)$$

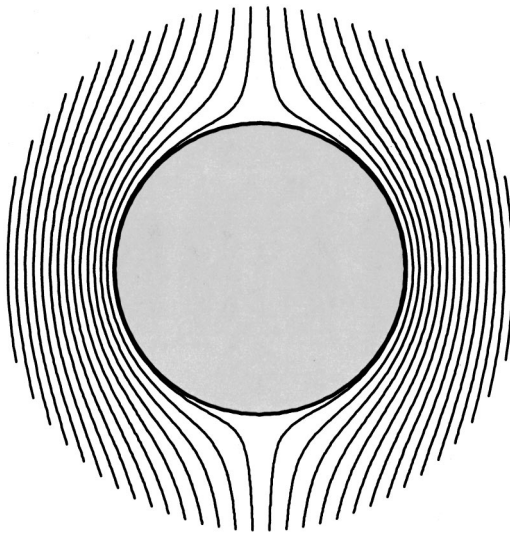


FIG. 1. RMF field lines, as they wrap around a perfectly conducting cylinder.

If we consider only the $n=1$ mode, we know that $B_\theta \rightarrow B_{\text{RMF}}$ as $r \rightarrow \infty$, and that if there were a perfectly conducting cylinder at $r=R$, then $A_z \rightarrow 0$, as $r \rightarrow R$. For this case $a_1 = -B_{\text{RMF}}$, and $\beta_1 = B_{\text{RMF}}R^2$, so

$$B_\theta = B_{\text{RMF}} \left(1 + \frac{R^2}{r^2} \right) e^{i\theta}. \tag{4}$$

In this case the RMF field magnitude (as represented by B_θ) increases to double its large radius value, as r decreases and approaches R . This increase results from the field lines wrapping around the conducting cylinder, as illustrated in Fig. 1.

On the other hand, a FRC is not a perfectly conducting cylinder, but it is still possible to calculate the RMF field between the containment wall and the FRC, assuming this region is a vacuum. If the RMF field at the vacuum vessel wall $B_{\theta\text{Wall}}$ is known, Eq. (3) can be used to write

$$B_\theta = \left(-\alpha + \frac{\beta}{r^2} \right) e^{i\theta}, \quad \alpha = -B_{\text{RMF}}, \tag{5}$$

$$\beta = -R_{\text{Wall}}^2 (B_{\text{RMF}} - B_{\theta\text{Wall}}).$$

Thus, if both B_{RMF} and $B_{\theta\text{Wall}}$ are known, Eq. (5) can be used to specify the RMF field between vacuum tube wall and the FRC (assuming this region is a vacuum). This equation allows the B_θ predicted by the MHD code, to be compared with the vacuum solution. Similarly, if B_{RMF} and $B_{\theta\text{Wall}}$ are measured in an experiment, it can be used to predict B_θ between the wall and the separatrix.

B. MHD simulation results

The numerical simulations reported in this paper employ parameters relevant to the Translation Confinement and Sustainment (TCS) experiment at the University of Washington.⁶ The details of the numerical model have been described elsewhere.⁴ The calculations are initialized with a B_z and n profile of a FRC in equilibrium. During the calculation, the FRC length is adjusted to maintain the average β

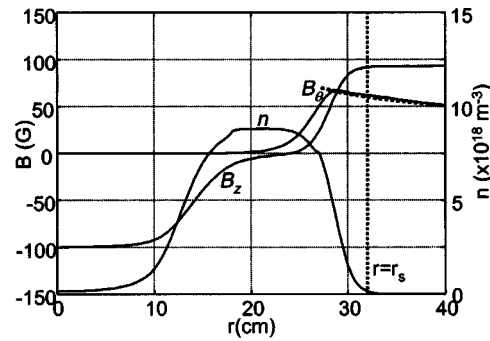


FIG. 2. Equilibrium magnetic and density profiles for the *standard* calculation.

condition and adjustments are made to maintain n , T , and P as a function of ψ , as described previously.⁴ The initial conditions for the *standard* numerical simulation of this section are a uniform temperature $T_{e0} = 30$ eV, external axial magnetic field $B_{z0} = 115$ G, and $x_s = 0.75$. The simulation region extends from $r = 0$ to $r = 40$ cm, and a flux conserving coil is at $R_c = 47$ cm. The RMF field ramps on in $1 \mu\text{s}$ to $B_{\text{rmf}} = 35$ G, and has a frequency $\omega_{\text{rmf}} = 1.1 \times 10^6 \text{ s}^{-1}$. A uniform resistivity of $125 \mu\Omega\text{m}$ is employed, and the plasma temperature is limited to values less than 30 eV.

A low minimum pedestal density n_{min} , is applied to circumvent numerical difficulties associated with the Hall term in the MHD equations. For the *standard* case, $n_{\text{min}} = 1.2 \times 10^{16} \text{ m}^{-3}$, which is approximately 0.1% of the peak equilibrium density. It will now be shown that the selection of this value can have a dramatic effect on the calculation—if it is too large.

Figure 2 shows the magnetic field and density profiles for the *standard* case after the calculation has reached equilibrium. The input value of B_{RMF} and the numerically calculated value of $B_{\theta\text{Wall}}$ have been used with Eq. (5) to calculate the vacuum solution for B_θ . The magnitude of this quantity is shown as a dashed line in Fig. 2. The B_θ profile calculated by the MHD code is seen to agree well with the vacuum prediction. Figure 3 shows the results from an identical calculation, except that n_{min} has been increased to $8.4 \times 10^{16} \text{ m}^{-3}$, which is about 0.7% of the peak equilibrium density. For this case the calculated B_θ profile rises significantly over the vacuum based prediction, which leads to greater penetra-

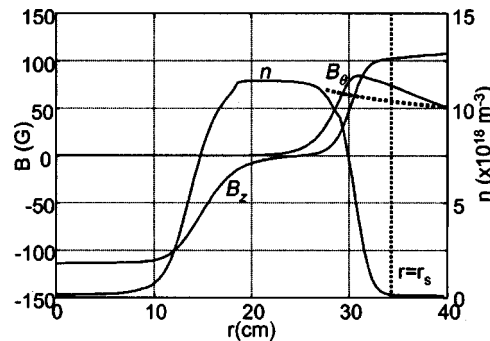


FIG. 3. Equilibrium magnetic and density profiles for a calculation where n_{min} has been increased to $8.4 \times 10^{16} \text{ m}^{-3}$.

tion. This is manifested through more driven current, as required to support the larger swing in B_z , higher density and pressure, and larger separatrix value.

This numerical result may seem somewhat contrived, since it depends upon the setting of an artificial pedestal density. However, mechanisms do exist for the creation of plasma near the vacuum vessel wall in experiments. The quartz wall is known to outgas, and could easily be a sufficient source of neutrals. For the calculation shown in Fig. 3, approximately 5.4×10^{16} ions per cm per s ($\text{cm}^{-1} \text{s}^{-1}$) were generated by the code to maintain the pedestal density. This density generation occurs in a thin annular region around the vacuum vessel wall. The particle production rate is sufficient to add about 2.5% of the FRC inventory in the 500 μs calculation. The power required to ionize this much plasma is miniscule—approximately 0.4 W/cm of length, when a total ionization cost of 50 eV per ion is assumed. This can be compared to a total Joule heating rate of about 7.75 kW/cm.

C. Physical understanding

In this section, the physical mechanism for RMF amplification in the open field line region is described. Here, the θ -dependence of the variables is represented spectrally as

$$q(\theta) = q_0 + \left(\sum_{n=1}^N q_n e^{in\theta} + \text{c.c.} \right). \quad (6)$$

The axial current J_z , in the open-field line region must be approximately in phase and in the same direction as the current in the RMF antennae. At first this may seem counterintuitive, since image currents are usually in the opposite direction and buck out the magnetic field. But if we consider the forces on the open-field line plasma, it becomes apparent why the RMF has to increase with decreasing radius from the wall. The total force on the plasma can be expressed as $(\mathbf{J} \times \mathbf{B}) - \nabla P$. Considering only the $n=0$ component of the radial force, and splitting the first term into its two spectral components yields

$$F_{r,0} = J_{\theta,0} B_{z,0} - 2 \operatorname{Re}(J_{z,1} B_{\theta,1}^*) - \frac{\partial P_0}{\partial r}, \quad (7)$$

where the $J_{\theta,0} B_{z,0}$ term represents the contribution from the $n=0$ component, and the $\operatorname{Re}(J_{z,1} B_{\theta,1}^*)$ represents the contribution from the $n=1$ component. Since the RMF quickly penetrates the low-density plasma in this region, the azimuthal current in this region is negative, and can be expressed as $J_{\theta,0} = nq_e \omega_{\text{RMF}} r$. The first term in Eq. (7) is thus negative, and will drive a radially inward fluid velocity until one of the other two terms is large enough to balance it. The inward radial velocity has two effects: (1) It evacuates the plasma from the region near the wall and that creates a pressure gradient that opposes the $J_{\theta,0} B_{z,0}$ term; (2) It convects the RMF inward, generating the RMF amplification. In this case $J_{z,1}$ is predominantly real and negative while $B_{\theta,1}$ is predominantly real and positive so $-2 \operatorname{Re}(J_{z,1} B_{\theta,1}^*)$ is positive, which is a radial force out.

It is instructive to evaluate the requirements for the pressure gradient to balance the $J_{\theta,0} B_{z,0}$ term. For simplification it is assumed that the temperature is constant. Then,

$$J_{\theta,0} B_{z,0} = nq_e \omega_{\text{RMF}} r B_z = k_B T \frac{\partial n}{\partial r},$$

which implies

$$\frac{\partial n}{\partial r} = \frac{q_e}{k_B} \frac{\omega_{\text{RMF}} r B_z}{T} n. \quad (8)$$

For the *standard* simulation case with $\omega_{\text{RMF}} = 1.1 \times 10^6 \text{ s}^{-1}$, $r = 0.40 \text{ m}$, $B_z = 0.0115 \text{ T}$, and $T = 30 \text{ eV}$. If we approximate $r B_z / T$ as constant in the annular region between the separatrix and the wall, the above equation implies that the density must decay as e^{-170r} in this region, or about 1 e -folding every 6 mm. Without an *external* source of plasma, this may be accomplished, and equilibrium established without radial flow on the open field lines. If there is a significant space between the plasma and the wall and no plasma source in this region, the wall density will be kept very low by this effect. However, if plasma is continuously generated, as represented by the pedestal density in the numerical simulations, the pressure gradient alone cannot balance the $J_{\theta,0} B_{z,0}$ term, and a radial flow causes RMF amplification until the second term in Eq. (7) grows until F_r is zero.

It is also instructive to estimate the requirements for the RMF to balance the $J_{\theta,0} B_{z,0}$ term. A rough estimate can be obtained by assuming that the change in magnetic pressure from the decrease in B_z is matched by an increase in the magnetic pressure from an increase in B_θ (over its vacuum solution). This can be expressed as

$$\Delta(B_z^2) = -\frac{1}{2} \Delta(B_\theta^2),$$

or, assuming ΔB is small compared to B

$$\Delta B_\theta = -\frac{2B_z \Delta B_z}{B_\theta}. \quad (9)$$

The term ΔB_z can be estimated from $\nabla \times \mathbf{B} = \mu_0 \mathbf{J}$, so

$$\Delta B_z \approx \mu_0 n e \omega_{\text{RMF}} r \Delta r. \quad (10)$$

For the simulation case with $n_{\text{min}} = 8.4 \times 10^{16} \text{ m}^{-3}$, $\omega_{\text{RMF}} = 1.1 \times 10^6 \text{ s}^{-1}$, $r = 0.40 \text{ m}$, and $\Delta r = 0.1 \text{ m}$, the above equation predicts a $\Delta B_z = 7.4 \text{ G}$. Then using $B_z = 115 \text{ G}$ and $B_\theta = 35 \text{ G}$, Eq. (9) predicts $\Delta B_\theta = 48 \text{ G}$ in approximate agreement with the simulation shown in Fig. 3. Equations (9) and (10) show that if the density is sufficiently low, or if the separatrix is close to the wall so Δr is small, the effect can vanish.

D. Consequences of RMF amplification

By comparing the results of Figs. 2 and 3, one may want to conclude that this effect is always beneficial. RMF penetration was more rapid and the resulting equilibrium had higher pressure and B_z when the pedestal density was higher. However, this calculation was carefully chosen, with an open field-line density sufficient for significant RMF amplification, but small enough for a quiescent equilibrium. In a third calculation n_{min} has been increased to $1.8 \times 10^{17} \text{ m}^{-3}$, which is about 1.5% of the peak equilibrium density. In this case the peak B_θ is about 115 G at 15 μs into the calculation, and penetration is rapid. In a previous paper⁴ it was shown that

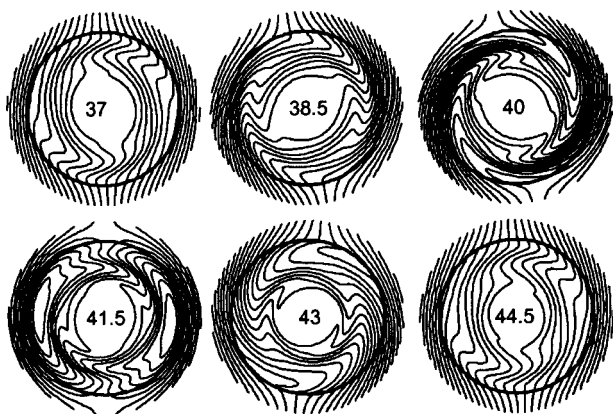


FIG. 4. Evolution of magnetic field lines during one rotation of the magnetic structure.

penetration continues until the penetration condition is almost satisfied, and a balance is achieved so that the RMF penetrates to the null, but not beyond it. The RMF amplification alters the penetration condition so that more current is driven in a higher density FRC. To support the increased current, the RMF must apply a larger torque to the electrons. If this exceeds the total torque that the RMF can supply, the entire magnetic structure inside the vacuum vessel begins rotating slower than the RMF. This is illustrated in Fig. 4, which shows the magnetic field lines at several times, projected onto the $r-\theta$ plane. Note that the graphs are plotted in a rotating frame of reference to make the external RMF appear vertical and stationary. The corresponding simulation time (μs) for each of the graphs is shown in its center.

The internal structure is rotating significantly slower than the RMF. In fact, in Fig. 4 the structure appears to have a period of $7.25 \mu\text{s}$, which means that its rotation frequency relative to ω_{RMF} is 0.87×10^6 . Thus the internal structure is rotating with a frequency of $\omega = 0.23 \times 10^6$, which is about 21% of ω_{RMF} . This is only an average rotation rate however, because the internal shape of the structure is seen to vary with its phase. In fact $u_{e\theta}$ is found to vary wildly as a function of radius and time during each rotation.

III. DISCUSSION AND SUMMARY

An important new physical effect that could have significant implications for the use of RMF current drive in a FRC has been investigated with a numerical model. It has been found that if there is a significant gap between the vacuum chamber wall and the FRC, and if the plasma density in this region is prevented from becoming arbitrarily low, then the RMF magnitude will grow with decreasing radius between the wall and the FRC. If conditions are such that the growth in RMF magnitude is modest, this effect can be beneficial by increasing the penetration rate and current drive efficiency. However, if the effect is too strong, the current drive efficiency is increased to a point where the torque required to maintain the electron rotation is too much for the RMF. In this case, the calculations predict the formation of a magnetic structure that rotates much slower than the RMF. The RMF

continues to drive the current with this structure, but the solution appears chaotic, and thus undesirable for FRC current drive. In addition, a significant plasma density is predicted all the way to the wall. This could be catastrophic in experimental plasma—especially if the RMF opens the FRC field-lines⁷ so there is direct parallel thermal conduction path to the wall.

The effect relies upon the existence of a mechanism to create new plasma near the vacuum chamber wall, however, the required plasma creation rates are well within realistic outgassing and ionization rates for experimental plasmas. However, it should be noted that we have neglected open field line losses due to axial flow. Inclusion of this effect would increase the required plasma production rate.

In the simulations presented here, the initial conditions include a very low density on the open field lines. It is natural to question whether this is important, particularly since this probably will not be true for planned experiments on TCS.⁶ If the simulation were initialized with a significant open field line density, but with a very low pedestal density, would RMF amplification take place, at least transiently during the initial RMF penetration? Calculations with a relatively high initial open field line density (10% of the peak density) showed that this change in initial conditions has almost no effect. During initial penetration, the RMF pushes this initial plasma ahead of it, quickly evacuating the outer radius region. This result has an additional significance, because it shows that the density outside of the FRC must quickly drop to a very low value, and that the RMF continuously sweeps plasma from this region. In the absence of a plasma source near the wall, Eq. (8) (or a variant of it that includes temperature variation) can be used to estimate the density near the wall.

Future work will include a comparison with experimental results. In particular, B_θ probe data will be analyzed and the magnitude compared with the vacuum solution to see if the amplification effect is evident, especially if FRCs with a significant gap between the wall and separatrix are formed. In addition, numerical and experimental probe signals will be carefully compared to ascertain whether internal rotating structures exist in the experimental device. Some initial results indicate that this is indeed true.⁶

ACKNOWLEDGMENTS

The author acknowledges many useful discussions with J. T. Slough, A. L. Hoffman, and H. Y. Guo during the course of this work.

The present work has been supported by grants from the Office of Fusion Energy Sciences of the U.S. Department of Energy.

¹L. R. Jones, Phys. Plasmas **6**, 1950 (1999).

²J. T. Slough and K. E. Miller, Phys. Plasmas **7**, 1945 (2000).

³J. T. Slough and K. E. Miller, Phys. Rev. Lett. **85**, 1444 (2000).

⁴R. D. Milroy, Phys. Plasmas **7**, 4135 (2000).

⁵W. N. Hugrass and R. C. Grimm, J. Plasma Phys. **26**, 455 (1981).

⁶H. Guo, A. Hoffman, J. Slough, B. Brooks, E. Crawford, and G. Votrubeck, Bull. Am. Phys. Soc. **45**, 247 (2000).

⁷S. A. Cohen and R. D. Milroy, Phys. Plasmas **7**, 2539 (2000).